3.1 Introduction

As we have already discussed in introduction section that Bi_2Te_3 is one of the most attractive element among A_2B_3 series (A=Bi, Sb and B=Te, Se), having n type of carrier density due to the large amount of Te vacancies. Hor et al. [43] who have reported superconductivity in Cu calcated Bi_2Se_3. Since Bi_2Se_3 and Bi_2Te_3 belong to the same A_2B_3 family therefore, it might be interesting to observe the effect of Cu in Bi_2Te_3 sample. Moreover, various studies have been performed towards the tuning of carrier type *viz.* Jo et al. have observed such type of phenomenon in Fe incorporated Bi_2Te_3 samples[31]. Additionally, Choi et al. have also reported such tuning in Bi_2Se_3 with the incorporation of Mn [32] whereas similar type of properties has been observed by Wang et al. with the introduction of Ca ions into the Bi_2Se_3 based topological insulators [33]. Interestingly, most of the reports in Bi_2Te_3 samples have been seen towards the doping on Bi-sites [31-33], while to the best of our knowledge doping on Te- site has not yet been observed which however might be equally interesting to study. Therefore, we have doped Cu towards the Te site in Bi_2Te_3 TI. Hall resistivity measurements clearly revealed the n to p-type tuning with Cu doping.

Furthermore, magnetic ordering in topological insulators may also open a new way towards the various promising applications in the emerging field of spintronics and many other novel phenomena such as magnetoelecric quantum states, magnetic monopole, and anomalous quantum Hall effect [1, 2]. Besides these exotic phenomenon, quantum oscillations in transport experiments i.e. Shubnikov–de Haas (SdH) oscillations may also play a key role in topological insulators which can be seen only at low temperatures and in high magnetic fields in very good quality crystals. Moreover, SdH oscillations are one of the

much effective tools to investigate the topology of the Fermi surface of both, bulk and surface which is a fundamental key for the study of the physical properties in the metals [39].The measurement accuracy in the determination of Fermi surface cross-sectional areas is better than 0.1% of the area of the Brillion zone whereas in case of effective masses accuracy, it is better than ~5% [39].

In this chapter, we have investigated the structural, magneto-transport and magnetic properties of Cu doped Bi_2Te_3 samples which was showing n to p-type tuning, high carrier concentration and mobility, large magnetoresistance and ferromagnetism, which are important for quantum computing, spintronics devices, multifunctional electromagnetic application and disc reading heads.

3.2 Results and Discussion

3.2.1 X-Ray Diffraction Analysis

Single crystals of $Bi_2Cu_xTe_{3-x}$ (x=0, 0.03, 0.09) with the cleaved surface along the basal planes were characterized using X-ray diffraction patterns collected at room temperature [Fig.3.1(a)]. X-ray diffracted beam directions showed only the (00L) i.e. (003), (006), (0015), (0018) and (0021) peaks, all indexed peak matched well with JCPDS card no-15-0863 with space group R-3m. Further confirmation of the single crystallinity nature of the samples has been done by Laue pattern experiment. Fig.3.2 displays the Laue pattern of entire samples (x=0, 0.03 and 0.09). Dot pattern of Laue experiment in all the samples is showing the excellent single crystalline nature. Around $2\theta=54^0$ and 64^0 [Fig. 3.1(a)], a small splitting due to the difference in the wavelength of X-ray source of CuK_α and CuK_β radiation has been observed. An additional peak around $2\theta=40^0$ for both the samples has been observed which might be due to the slight misalignment or slight tilt angle of the crystallinity

of as cleaved single crystals. The change of lattice parameter and FWHM value evidences that Cu clearly substituted to Te in Bi_2Te_3 sample. The Full Width Half Maxima (FWHM) of the (003) peaks for the pure sample was as small as (~$0.0960^0 \pm 0.0014^0$) indicating that as

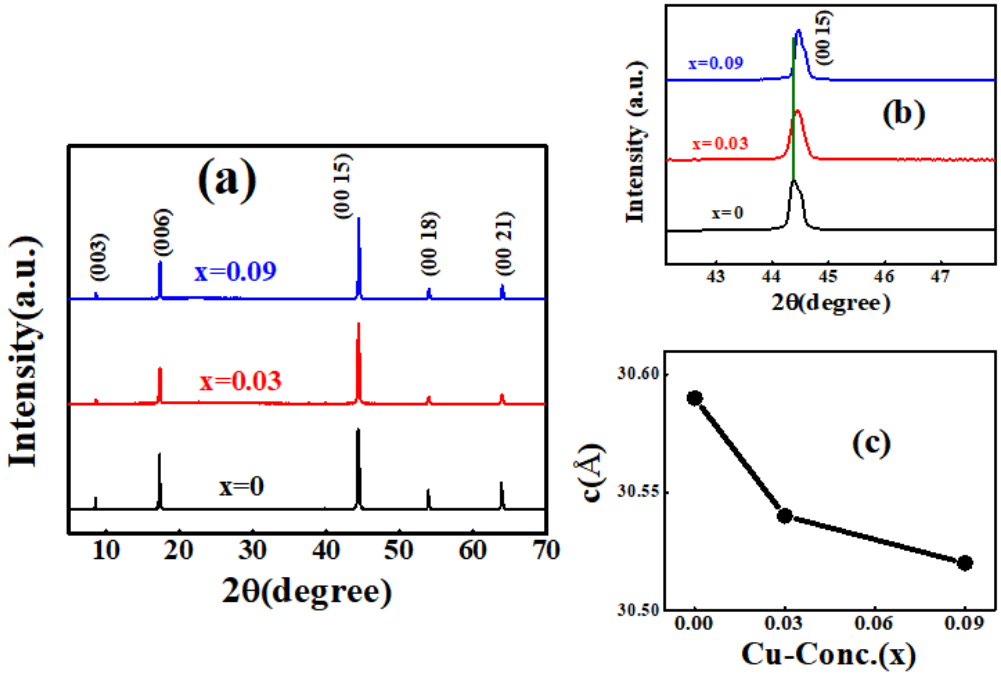

Fig.3.1 (a) XRD pattern of as prepared $Bi_2Cu_xTe_{3-x}$ (x=0, 0.03, 0.09) (b) Zoom portion of (00 15) peak, (c) Variation of lattice parameter 'c' as a function of doping concentration x.

Prepared sample has excellent single crystallinity in a long range. With increasing Cu concentration, the FWHM value has been found to increase and hence resulting a lowering of the crystallites size. Moreover a small shift towards higher angle in 2θ value with the doping of Cu in the doped sample [shown in Fig. 3.1(b)] is clear evidence that the lattice parameter is decreasing with Cu doping. The obtained c parameters for pure Bi_2Te_3 sample is 30.59(0) Å and with increasing x, it slightly decreases finally going to 30.52(1) Å for x=0.09 [shown in Fig. 3.1(c)], which well matched with the reported values [31]. Since the ionic radius of Cu is less than the Te hence the decrease in lattice parameter c results with the increase in doping concentration of Cu in the doped samples.

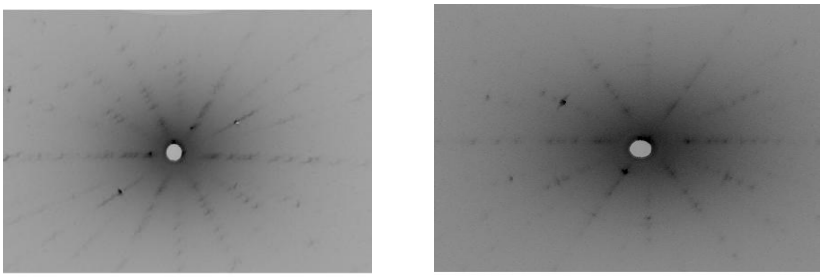

x=0 **x=0.03**

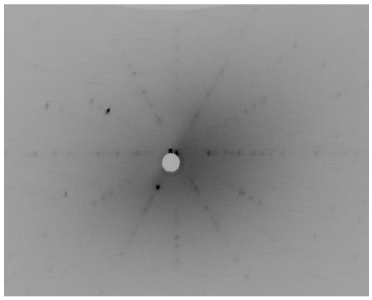

x=0.09

Fig.3.2 Laue pattern of the single crystals $Bi_2Cu_xTe_{3-x}$ (x=0, 0.03, 0.09).

3.2.2 Electrical Resistivity

Variation of longitudinal resistivity (ρ_{xx}) as a function of temperature under different magnetic field for the samples x=0, 0.03 and 0.09 has been shown in Fig. 3.3. It is clear from the graph that the value of resistivity is increasing as we are increasing Cu concentration; this is because of extra scattering centre created due to Cu. Scattering centre will increase with the increasing concentration of Cu. It is clear from the graph that the samples x=0 and 0.03 are showing positive temperature coefficient for the entire range of measurement temperature, no anomaly has been seen for both of the samples.

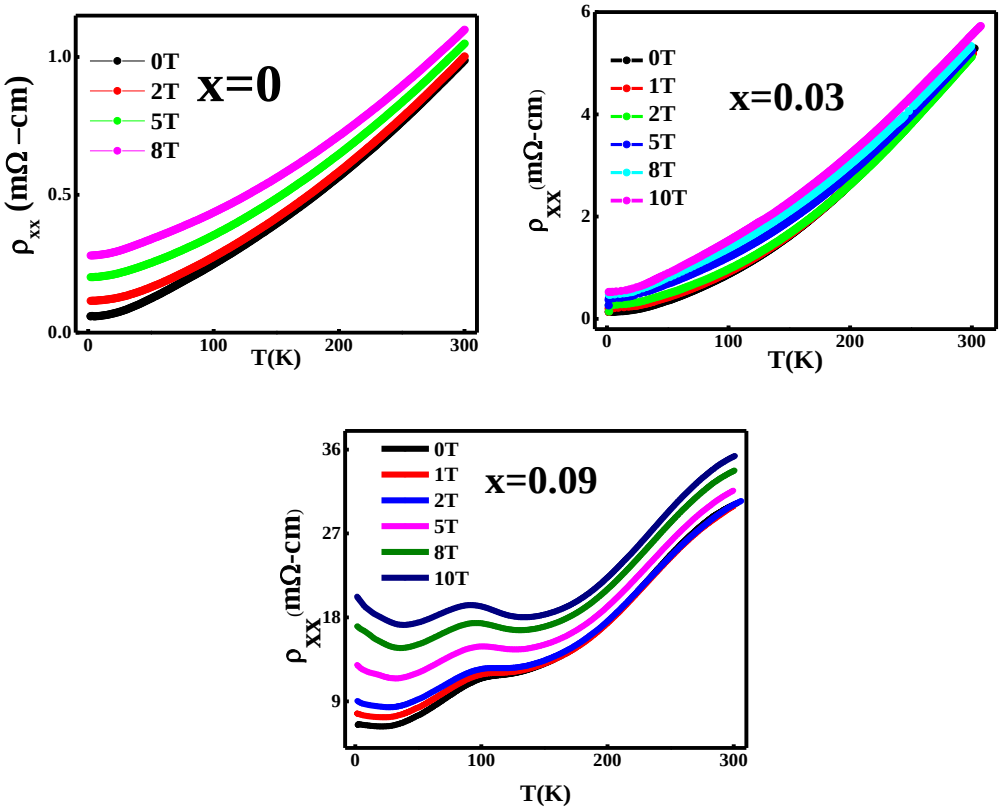

Fig.3.3 Variation of resistivity as a function of temperature at different magnetic field for the samples $Bi_2Cu_xTe_{3-x}$ (x=0, 0.03, 0.09).

This characteristic temperature dependence of the ρ_{xx} suggests the presence of surface metallic conduction for the whole range of measurement temperature and field for both of the samples, indicating that the topological surface is robust for the presence of low concentration of Cu. It should be noted that there is a marked difference in the nature of longitudinal resistivity for the sample x=0.09. It is obvious from the graph that there is drastic change in the nature of resistivity curve for this sample and we can easily observe anomalies at different temperatures. Moreover anomalies become more significant at higher fields shown in the Fig. 3.3. In x=0.09 sample anomalies are located at 35K, 90K and 140K. Earlier report suggests the presence of metallic behavior only in the low temperature region below 150K, above this temperature bulk insulating behavior dominates over surface metallic behavior [46-48] but in our case for x=0.09 sample, temperature coefficient is positive

showing metallic nature even at high-temperature region above 150K. No signature of negative temperature coefficient has been seen in x=0.09 sample even at higher temperature region indicating the presence of surface metallic behavior which is in contrast with the reported value [46-48].The saturation of resistivity ρ_{xx} around 90K in x=0.09 sample indicates a finite metallic conductivity [46-48]. Weak upturn below 35K and 140K in x=0.09 sample has been found. Such type of upturn has been seen in some other reports [46, 48] which origin is still not clear and further study is needed.

3.2.3 Hall Analysis

For the determination of the carrier concentration (*n* or *p*) and mobility (μ) of the samples $Bi_2Cu_xTe_{3-x}$ (x=0, 0.03, 0.09), we have performed Hall measurement at different temperatures, using the slope of the Hall resistivity we have determined the carrier concentration of the Samples. Figs. 3.4 (a, b, c) show the variation of Hall resistivity as a function of applied magnetic fields for the samples x=0, 0.03 and 0.09 at different temperatures. It is clear from the graph that slope of the curve is negative which indicates about the n type carriers for x=0 sample, it is noteworthy that slope changes its nature from negative to positive in the Cu doped samples(x=0.03 and 0.09) showing that carriers are tuned from n type to *p* type in the doped samples for the entire range of temperature of measurement. Generation of electrons by Te_{Bi} antisite defects in pure sample might be a reason for the tuning of charge carriers [31]. Moreover, it is clear from Figs. 3.4 (a, b, c) that sample x=0 is showing linear but samples x=0.03 and 0.09 were showing non linear behavior in Hall graph which might be an indication of quantum anomalous Hall Effect (QAHE) and presence of ferromagnetism in doped samples. Variation of bulk carrier concentration (N) as a function of temperature has been shown in Inset I of Figs. 3.4(a, b, c) for the samples x=0,

0.03 and 0.09 respectively. The estimated carrier concentration well matched with the reported values in TIs [30, 34, 49]. It is clear from carrier concentration (N) vs. temperature (T) graph that carrier density increases with the increase in temperature which might be due to the fact that at high temperature bulk contribution dominates over surface contribution results in the enhancement in the carrier concentration. In fact,

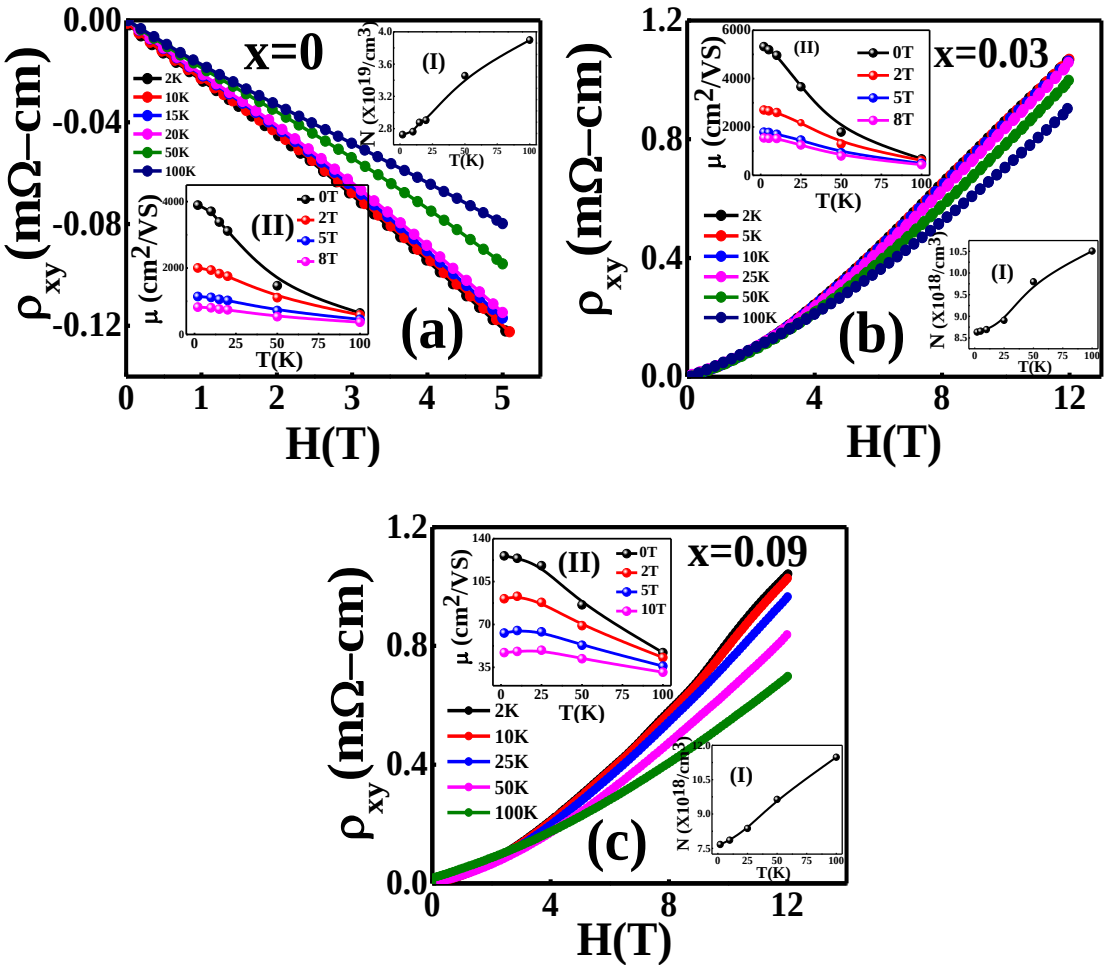

Fig.3.4 (a, b, c) Variation of Hall resistivity with applied magnetic field at different temperatures for the samples $Bi_2Cu_xTe_{3-x}$ (x=0, 0.03, 0.09) respectively, Inset I is showing variation of carrier concentration as a function of temperature whereas Inset II is showing variation of carrier mobility with temperature at different applied magnetic field for respective samples.

Topological surface state is a complete quantum phenomenon and as a matter of fact, surface effect will be significant at very low temperature. In consequence, at very low temperature

surface state dominates over bulk state and that is why the carrier concentration is low at low temperature (T≤20K) and very large at high temperature. Moreover, the rate of increment of carrier density is also increasing with the increase of temperature confirming the dominance of bulk insulating character over surface metallic character at higher temperature.

Using the data of carrier concentration and electrical resistivity we determined bulk carrier mobility of the samples. The calculated mobility (μ) of the carriers well matched with the reported values in the TIs [32, 49], variation of mobility with temperature at different applied field *viz.* 0T, 2T, 5T and 8T have been shown in inset II of Figs. 3.4(a, b, c) for the samples x=0, 0.03 and 0.09 respectively. It is obvious from the graph that as we increase both the temperature and field, mobility decreases for the entire sample which might be due to the freezing out of phonons with decrease of temperature and also with the increase of magnetic field.

High conductivity of Cu and production of scattering centre due to the doping of Cu in Bi_2Te_3 sample may be the two major factors for the mobility. It is noteworthy that when we doped Cu in Bi_2Te_3 sample, carrier concentration is decreasing and mobility is increasing for the initial concentration of Cu(x=0.03) which might be due to the high conductivity of Cu since conductivity of Cu is very high than pure Bi_2Te_3 , Cu produces a perculation path in the movement of carriers hence high mobility results but when we further increased the doping of Cu (x=0.09), scattering centers due to the Cu becomes dominating factor hence low mobility results.

3.2.4 Magnetoresistance Analysis

Variation of magnetoresistance with applied magnetic field for the samples $Bi_2Cu_xTe_{3-x}$ (x=0, 0.03, 0.09) has been shown in the Figs.3.5(a, b, c) respectively.

Magnetoresistance (MR) of the samples has been defined as, $MR\% = \frac{R(H)-R(0)}{R(0)} X 100\%$ where R(H) is the resistance at applied magnetic field H, R(0) is the measured resistance at H=0. It is obvious from the MR graph that it is completely symmetric for all the samples with respect to the reversal of the magnetic field direction, ruling out any possible contribution from Hall voltage. MR for all the samples increases with applied field but decreases with increasing temperature. Increasing carrier concentration with temperature may be a reason for the decreasing MR value. For x=0 sample, It is clear from Fig. 3.5(a) that MR behaviour is linear up to the measured field, no signature of oscillation has been observed. But for the sample x=0.03 and 0.09 quantum oscillation can be clearly observed. Several groups already studied the Magnetoresistance experiment in pure Bi_2Te_3 [36, 50, 51, 52]. So here we have focussed only on the study of topological surface state of Cu doped Bi_2Te_3 samples. It is obvious from the MR curve that at low temperature a dip in MR is observed for the Cu doped samples x=0.03 and 0.09, which might be due to the existence of weak antilocalization (WAL) [50]. Above the Dirac point, an electron on the surface moving in a circular path will possess a π berry phase however the spin of electron will be rotated by 2π and the interference of the pair of the time reversed paths changes from constructive to destructive due to this π berry phase [37] hence 2D WAL effect results from the surface of topological insulators which is in good agreement with our results [shown in Figs. 3.5(b and c)]. Moreover it is observed from the MR curve that as we increase temperature, MR dip broadened at low field because at higher temperature phase coherence length decreases [50]. As we increase temperature, MR becomes linear for intermediate temperature range and again at higher temperature i.e. 300K it is showing quadratic behaviour. Wang et al. [36] has also observed similar type of quadratic growth behaviour without any sign of saturation at

high temperature in Bi_2Te_3 film. We can easily observe oscillations in the field dependent resistivity graph at low temperatures and high magnetic field in both of the Cu doped samples x=0.03 and 0.09 [shown in Figs. 3.5 (b, c)] respectively, however the oscillations are more prominent in the case of x=0.09, such type of oscillations in the magnetoresistance in metals are known as Shubnikov de-Hass (SdH) oscillations. Here the magnetic field has been

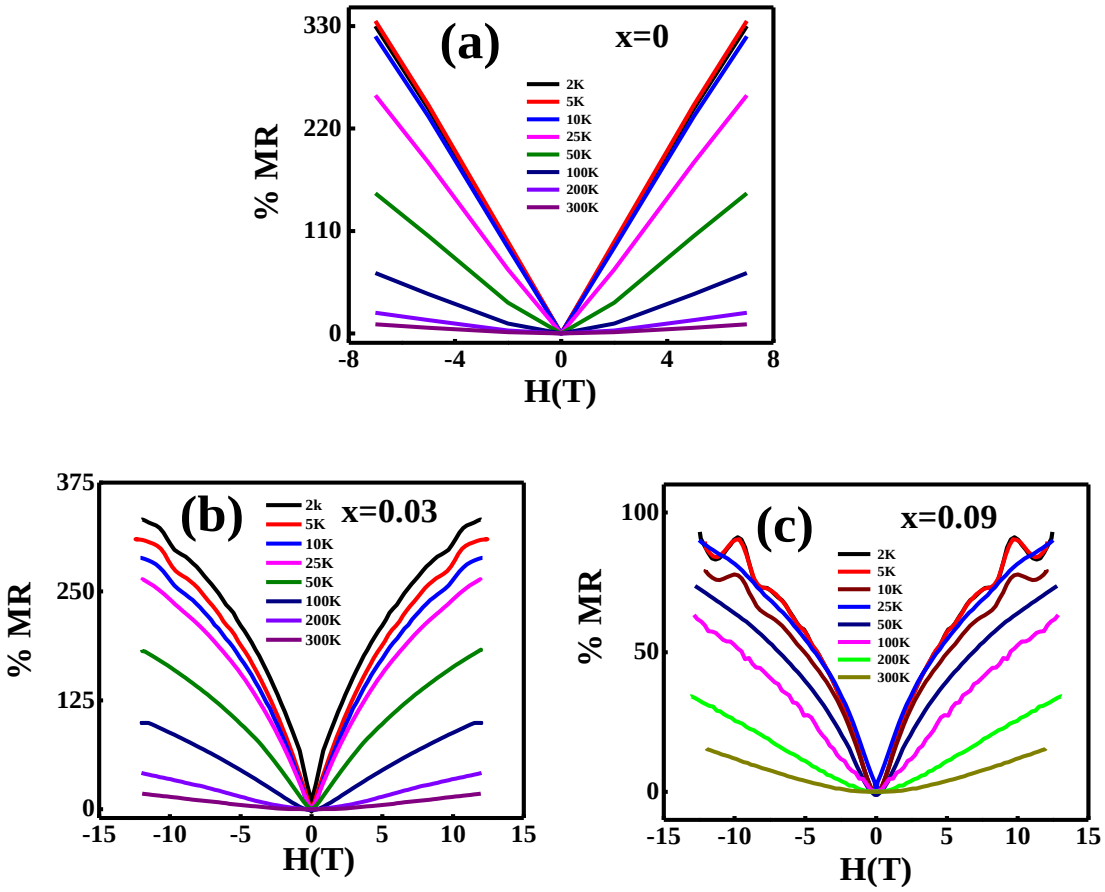

Fig.3.5 (a, b, c) Variation of magnetoresistance as a function of applied magnetic field under different temperatures for the samples x=0, 0.03 and 0.09 respectively.

applied perpendicular to the surface of the cleaved crystal. In this portion we now turn to focus only on the samples having oscillations (x=0.03 and 0.09) and discuss the surface metallic behaviour. In order to see the clear quantum oscillations in the samples, $d\Delta R_{xx}$ at different temperatures viz 2K, 5K, 10K, 25K and 50K have been plotted as a function of

inverse magnetic field B^{-1} shown in of Fig.3.6(a) for the sample x=0.03 [ΔR_{xx}has been found by subtracting the smooth polynomial background from R_{xx}].It is seen that amplitude of the oscillations decreases with the increase in the temperature but there is no change in frequency [shown in Fig. 3.6(a)]. The presence of TSSs can be further confirmed

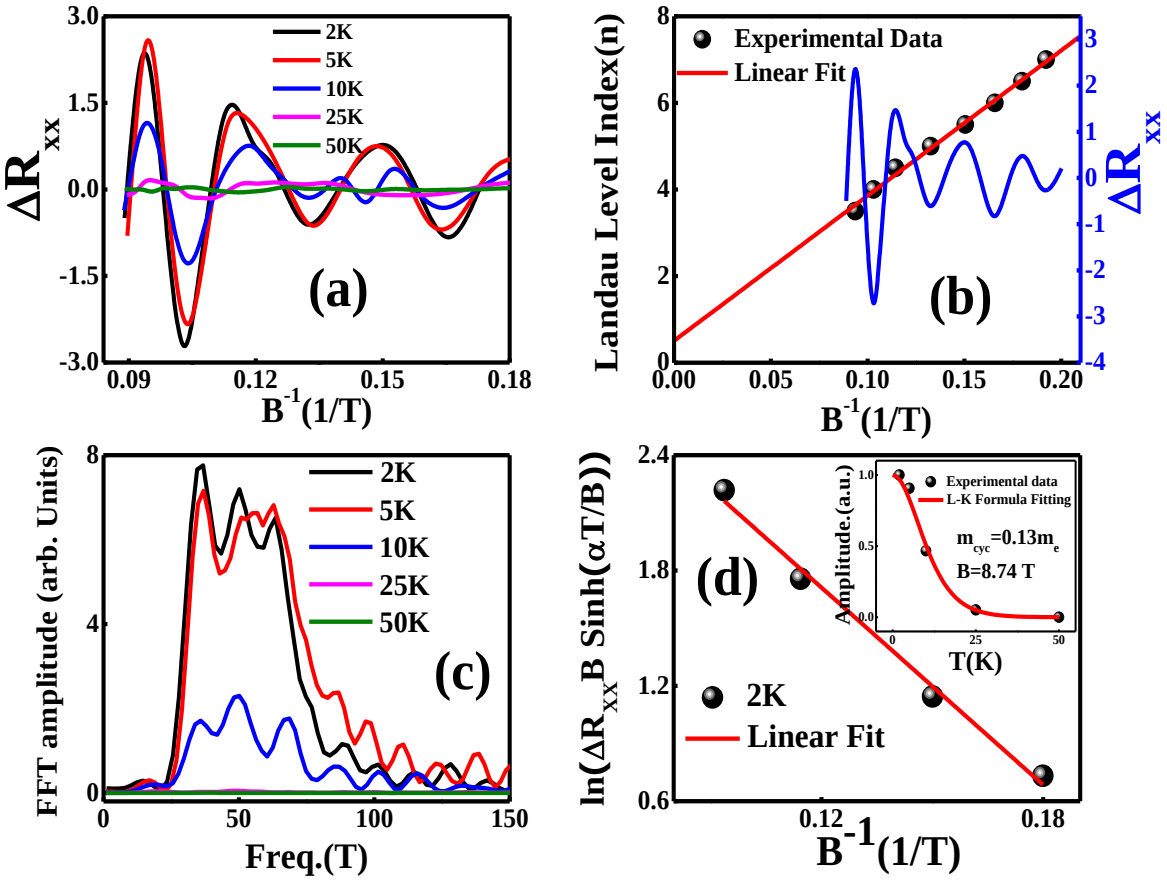

Fig.3.6 Study of SdH oscillation for the sample x=0.03 (a) SdH oscillations plotted against 1/B at different temperatures. (b) SdH oscillations and Landau levels with inverse magnetic field and linear fitted curve (red line). (c) The FFT corresponding to Fig. (a); (d) Fit to the Dingle damping term at 2K with the resulting Dingle temperature T_D=9K, Inset show the L-K fitting of the SdH oscillation and obtained cyclotron mass (m_c) 0.13 m_e from fitting, at applied field 8.74T

by the value of Berry phase β which can be obtained by the Landau level fan diagram where the inverse magnetic field values at which maxima and minima ($1/B_{max}$and$1/B_{min}$) occurs is plotted as a function of integer n, known as the n^{th} Landau level. We have used the relation $n=F/(2\pi B_n)+\beta$. Here the minima in resistivity correspond to n whereas maxima correspond to

(n+1/2) and F is the frequency. The value of β=0 and ½ indicates about normal fermions and Dirac fermions respectively. We can obtain the value of β by the linear extrapolation of 1/B tends to zero which is known as the value of Berry phase. In Fig. 3.6(b) black spheres are showing the Landau level fan diagram for the sample x=0.03 at 2K and red line is showing the linear fit. The extracted value of β is 0.51, which is very close to ½ which indicates that the oscillations originate from the surface helical state. Moreover, we have obtained the oscillating frequency (F) from the slope of Landau level fan diagram, the circular assumption $A=\pi k_f^2$ allowed us for the determination of Fermi momentum (K_f) and the obtained value of K_f was 7.99×10^8 m^{-1} which well-matched with the reported value in TIs [37,46,52].We have determined Fermi surface cross section (A) from the Onsagar's relation $F=\hbar A/(2\pi e)$, the calculated surface carrier concentration is $n_s=k_f^2/2\pi=5.1\times10^{12}/cm^2$ if we assume that k_f corresponds to a two - dimensional (2D) Fermi surface , however the calculated bulk carrier concentration is $n_b=k_f^3/3\pi^2=1.7\times10^{18}/cm^3$ if we assume that k_f corresponds to a three - dimensional (3D) Fermi surface. The value of calculated carrier concentration is in good agreement with the carrier concentration from the Hall measurement discussed above.

To identify the origin of the oscillations, we have also performed fast Fourier transforms (FFTs) [shown in Fig. 3.6(c)] at different temperatures corresponds to Fig. 3.6(a) for the sample x=0.03. FFT amplitude decreases with the increases in temperature. It is clear from fig.3.6(c) that only one prominent frequency is observed at 35T, peaks around 50T and 68T have been also observed, peak corresponds to 50T may be due to the presence of second channel which is very nearer to the channel corresponds to the 35T, whereas peak corresponds to 68 may be second harmonics of 35T. Other peaks with low intensity could be easily seen on the high field side of this frequency, small contribution from higher frequency

might be a reason for the presence of these peaks, but the effect is minor and disappears as we increase temperature, such type of effect has also been observed in some other TIs with complex Fermi surfaces [53-55].

The cyclotron mass has been determined from the temperature dependence of the oscillations which are observable up to~50 K as shown in Fig. 3.6(a). We have obtained the oscillation amplitude from the different peaks of ΔRxx for different temperatures (viz. 2K, 5K, 10K, 25K and 50K) at a constant magnetic field (viz.6.03T, 8.74T, 9.69T and 10.67T respectively). To obtain cyclotron mass at different fields mentioned above, we have also fitted the thermal damping factor of Lifshitz-Kosevich (LK) equation $R_T = (\frac{\alpha T}{B})/\sinh(\frac{\alpha T}{B})$ at 2K where $\alpha = (\frac{2\pi^2 k_B m_{cyc}}{e\hbar})$. L-K fitting corresponding to applied field B=8.74T has been shown in inset of Fig. 3.6(d); solid line is showing the fit using the L-K theory. The obtained m_{cyc} was $0.10m_e$, $0.13m_e$, $0.15m_e$ and $0.15m_e$ for the applied field 6.03T, 8.74T, 9.64T and 10.67T respectively, the average cyclotron mass obtained using these values found to be $m_{cyc} = 0.13m_e$, where m_e is the rest mass of an electron.

Using the oscillating frequency obtained from FFT , We have determined Fermi surface cross section (A) from the Onsagar's relation mentioned above, using the circular assumption, the determined k_f value was $3.30\times10^8 m^{-1}$, the calculated surface carrier concentration is $n_s=k_f^2/2\pi=8.69\times10^{11}/cm^2$ if we assume that k_f corresponds to a two - dimensional (2D) Fermi surface , however the calculated bulk carrier concentration is $n_b=k_f^3/3\pi^2=1.21\times10^{18}/cm^3$ if we assume that k_f corresponds to a three - dimensional (3D) Fermi surface. The value of calculated carrier concentration is in good agreement with the carrier concentration from the Hall measurement as well as Landau level fan diagram discussed above.

We have used the linear dispersion relation for the surface state $v_F = hk_F/2\pi m_{cyc}$, the calculated Fermi velocity was $v_F = 2.95\times10^5 ms^{-1}$. Following the standard Dingle temperature analyses Dingle temperature (T_D) at T=2K has been deduced from the fitting, yielding T_D= 9K [shown in Fig. 3.6(d)], and with the value of this calculated T_D the estimated surface carrier life time from $\tau = h/(4\pi^2 K_B T_D)$ was 1.36×10^{-13}s. Similarly, we have also calculated the mean free path $l = v_F\tau$ and surface quantum mobility $\mu = e\tau/m_{cyc}$ as 40nm and 239cm^2/Vs respectively. The obtained Fermi energy using the formula $E_F = m_{cyc}v_F^2$ is found to be 80 meV. It is obvious that the mobility calculated here is in consistent with the Hall mobility; hence one can conclude that the SdH oscillation is certainly coming from surface. These obtained physical parameters have good agreement to those already reported on other topological systems [37].

We have determined parameters corresponding to the x=0.09 sample also (shown in Fig. 3.7). Quantum oscillation at different temperatures has been shown using the variation of ΔR_{xx} as a function of inverse magnetic field presented in Fig. 3.7(a). It is obvious from the graph that amplitude of the oscillations is decreasing with the increase in the temperature which is similar to the x=0.03 sample. Berry phase obtained from Landau level fan diagram for x=0.09 sample was β=0.59 which clearly indicates about the Dirac fermions i.e. oscillations originate from the surface helical state.The calculated Fermi momentum (K_f) from Landau level fan diagram was 8.43×10^8 m^{-1} which well-matched with the reported value in TIs [37, 52, 46]. The estimated surface and bulk carrier concentration using Landau level fan diagram was $n_s = 5.6\times10^{12}$/cm^2 and $n_b = 2.0\times10^{18}$/cm^3 respectively for the sample x=0.09 which well matched with the carrier concentration obtained from Hall analysis. The oscillating frequency determined form FFT for x=0.09 sample was 33.5T which is very close

to the value obtained for x=0.03 sample [Fig. 3.7(c)]. It is clear from the graph that as we are increasing temperature, amplitude of FFT is decreasing, this behavior is similar to the previous case in x=0.03 sample. Using the L-K formula fitting, the calculated cyclotron mass (m_{cyc}) at the applied field 7.63T, 8.56T, 9.55T and 10.74T was $0.23m_e$, $0.15m_e$, $0.16m_e$ and $0.23m_e$ respectively. The average calculated cyclotron mass (m_{cyc}) for the sample x=0.09 was 0.18me [shown in Inset of Fig. 3.7(d)] which is higher than the previous case x=0.03 sample,

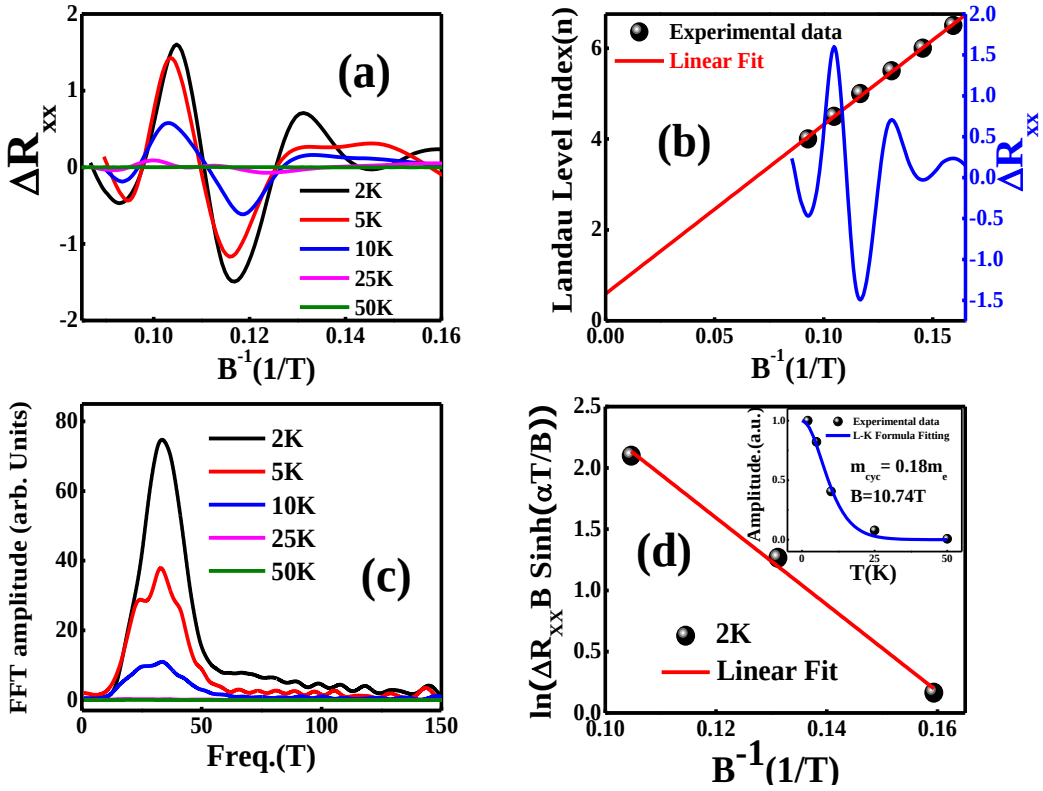

Fig.3.7 Study of SdH oscillation for the sample x=0.09 (a) SdH oscillations plotted against 1/B at different temperatures. (b) SdH oscillations and Landau levels with inverse magnetic field and linear fitted curve (red line). (c) The FFT corresponding to Fig. (a); (d) Fit to the Dingle damping term at 2K with the resulting Dingle temperature T_D=13K, Inset show the L-K fitting of the SdH oscillation and obtained cyclotron mass (m_c) 0.18 m_e from fitting, at applied field 10.74T.

that might be due to the increasing surface effect in x=0.09 sample since the SdH oscillations become more prominent in this sample as compared to x=0.03 sample which is clear from the Fig. 3.5. The estimated k_f, n_s and n_b from FFT were 3.18×10^8 m^{-1}, $8.05\times10^{11}/cm^2$ and

$1.09\times10^{18}/cm^3$. The values are slightly lower than the obtained values from FFT in x=0.03 sample which is due to the lower oscillating frequency in x=0.09 sample. The calculated T_D [shown in Fig. 3.7(d)], surface carrier lifetime τ, mean free path *l* and Fermi energy E_F were 13K, 9.12×10^{-14} sec, 19 nm and 43meV respectively. The calculated Fermi velocity v_F and surface quantum mobility μ was 2.01×10^5 ms^{-1} and 160 cm^2/Vs respectively, the lower value of v_F and μ is a clear evidence of the increasing surface effect in x=0.09 sample. The trend of decreasing value in mobility with increasing Cu concentration is similar to the trend obtained from Hall measurement.

3.2.5 Magnetic Analysis

In the systems similar to topological insulators, it is believed that the magnetic interactions mediated through charge carriers are responsible for raising ferromagnetism. Co, Fe and Mn doped magnetic TIs has been studied by different group [1, 2, 31, 32]. Though, exact explanation to the origin of ferromagnetism in topological insulators still requires more efforts. Since the pure Bi_2Te_3 is well reported diamagnetic material hence we will focus mainly on Cu doped samples x=0.03 and 0.09. In the current system of Cu doped Bi_2Te_3 topological insulator we have investigated detailed magnetization study by varying temperature and field. Fig 3.8, showing the temperature variation of susceptibility (χ) curves (x=0.03 and 0.09) recorded with an applied field of 1000 Oe followed by zero field cooled (ZFC) protocol. For the sample x=0.03, the susceptibility having a negative value~ -3.6×10^{-7} emu/g-Oe (at 300K) increases with decreasing temperature and at very low temperature~4K becomes positive by showing an abrupt rise in its value, fig.3.8(a). The negative value of susceptibility is clearly suggesting the existence of dominant diamagnetic nature of the sample for almost the whole temperature range except the lower temperature upturn (<4K)

where it takes positive value. The Bi_2Te_3 is now a well studied purely diamagnetic system, hence the dominant diamagnetic nature in the x=0.03 sample is not surprising but the lower temperature positive value of χ indicates towards induced magnetic properties in the system. The χ (T) curve for x=0.09 sample showing the susceptibility has been increased by an order ~-3.0×10^{-6} emu/g-Oe (at 300K) thus diamagnetism is seen to be diminished appreciably with increased Cu substitution, fig. 3.8 (b). Below 12K, the χ (T) crosses the zero line and becomes positive which is again an indication towards inducing ferromagnetism with Cu doping.

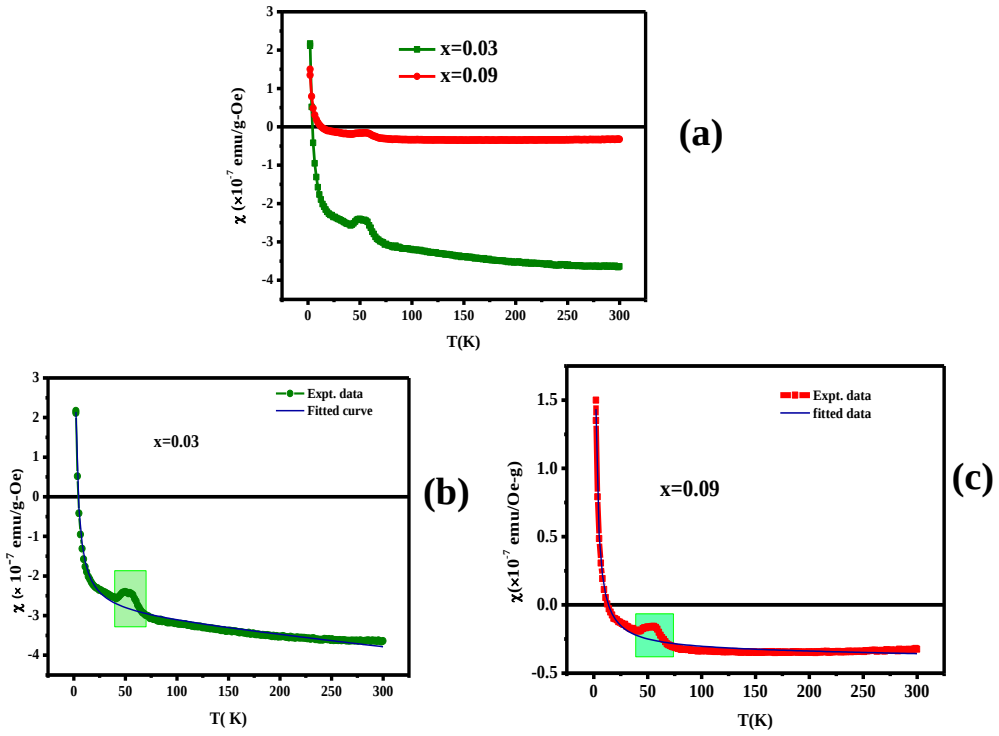

Fig. 3.8 Susceptibility (χ) vs. Temperature (T) curves at an applied field of 1000 Oe for the samples x=0.03 and 0.09. Figs. (b and c) showing individual fitted curves for the samples x=0.03 and 0.09.

Thus Cu substitution has shown to induce ferromagnetism effectively in the system TI $Bi_2Te_{3-x}Cu_x$. It is relevant here to mention that around temperature 50K, an anomaly in magnetization is observed for both the x=0.03 and 0.09 samples. The anomaly might be

related to the diamagnetic contribution. However, for quantitative analysis of diamagnetic and magnetic contribution, all the susceptibility curves can be fitted successfully by the following expression $\chi(T)= \chi_0 + D\times T + C/(T+\theta)$, here the first two terms are associated to the diamagnetic contribution while the third term is describing the standard modified Curie-Weiss law for magnetic spins interacting with each other. It can be seen from the figure. 3.8 (b & c) both of the curves were well fitted by the equation and the values obtained through the above fitting for the curves have been summarized in table 3.1.

Table-3.1: Different parameters obtained from susceptibility curves of samples x=0.03 and 0.09.

x	χ_0	D	C	θ
0.03	-2.98×10^{-7}	-2.84×10^{-10}	1.71×10^{-6}	+1.35
0.09	-3.41×10^{-8}	-1.01×10^{-11}	4.94×10^{-7}	+0.78

It can be noted that for x=0.03 sample the Curie-Weiss temperature θ is positive~ +1.35 K, indicating antiferromagnetic nature of the sample. While for higher concentration of Cu in x=0.09 sample, the Curie-Weiss temperature θ still remains positive but shows a decreased value +0.78K, suggesting decrease in antiferromagnetic contribution.

However, to further investigate the magnetic properties, we have performed field dependent isothermal magnetization study at temperature 2K. Fig. 3.9 showing the magnetic field (H) variation of magnetization (M) curves for the samples x=0.03 and 0.09. For the x=0.03 sample, the ferromagnetic nature is visible in the low field region (+/- 6000 Oe) but diamagnetic contribution starts appearing at higher fields which is typically associated to the dominant diamagnetic contribution of Bi_2Te_3 matrix. Evidently, for x=0.09 sample, the diamagnetic contribution in the M-H loop becomes very feeble which was indeed expected from previous M-T data analysis. Again, a closer view to the M-H loops reveal sizeable

increase in coercivity as well as the remnant magnetization with increasing Cu doping. The rise of ferromagnetism with increasing Cu substitution confirms that Cu is playing the crucial role in producing magnetic properties. Further study is needed for the exact origin of the induced ferro-magnetization.

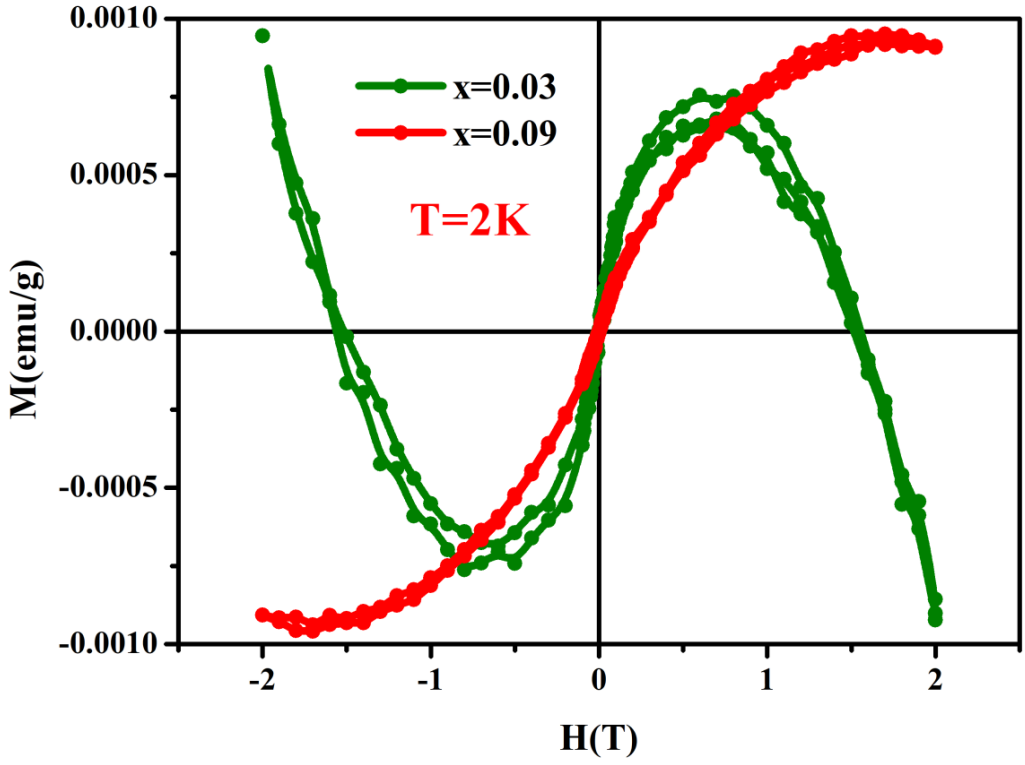

Fig. 3.9 M-H curves at 2K for the samples x=0.03 and 0.09.

3.3 Conclusion

In conclusion, we have investigated the structural, transport and magnetic properties of Cu doped Bi_2Te_3 topological insulators. With Cu doping, resistivity increases which may be due to the extra scattering centers produced due to Cu. It is also observed that Cu doping tunes the carrier from *n* to *p* type which is attributed due to the Te_{Bi} and Bi_{Te} antisites effects. Subnikov de Hass oscillation has been studied in the Cu doped samples. It is also seen that Cu is inducing ferromagnetism in Bi_2Te_3 sample which origin is still not clear.